EVALUATION OF AN ADAPTIVE UNSTRUCTURED REMESHING TECHNIQUE FOR INTEGRATED FLUID-THERMAL-STRUCTURAL ANALYSIS

PRAMOTE DECHAUMPHAI

FEBRUARY 1990

NASA
National Aeronautics and
Space Administration

Langley Research Center
Hampton, Virginia 23665

EVALUATION OF AN ADAPTIVE UNSTRUCTURED REMESHING TECHNIQUE FOR INTEGRATED FLUID-THERMAL-STRUCTURAL ANALYSIS

Pramote Dechaumphai*
NASA Langley Research Center
Hampton, Virginia

Abstract

An adaptive unstructured remeshing technique is evaluated for integrated fluid-thermal-structural analysis. The technique is combined with the finite element method to solve: (1) the Navier-Stokes equations for high-speed compressible flow, (2) the energy equation for the structural-thermal response, and (3) the quasi-static equilibrium equations for the structural response. The remeshing technique and the analysis solution procedure are described. The effectiveness of the approach is evaluated with two application studies. The flow analysis of Mach 8 shock-shock interference on a three-inch-diameter cylinder is used as the first application study to demonstrate the capability of the remeshing technique and to examine proper remeshing indicators for the inviscid and boundary layer regions. The applicability of the approach for the thermal and structural analyses of the structure is evaluated in the second application study of a 0.25-inch-diameter convectively cooled leading edge subjected to intense aerodynamic heating. Issues associated with remeshing indicators for thermal stress problems are identified.

Nomenclature

A	coolant passage area, Eq. (5), or finite element area, Eq. (10)
[A*]	Jacobian matrix, Eq. (8)
[B]	viscous flux matrix, Eq. (11)
c	specific heat, Eq. (4), or material elastic constants, Eq. (18)
E, F	x and y flux components
H	load vector, Eq. (3)
h	convective heat transfer coefficient, Eq. (5), or element spacing parameter, Eq. (22)
[I]	identity matrix
[K]	stiffness matrix
k	thermal conductivity
l, m	components of unit normal vector
$\dot{m}$	coolant mass flow rate
[M]	mass matrix
[N]	element interpolation or weighting function
$\bar{n}$	unit normal vector
P	coolant passage perimeter
p	pressure
q	heat flux
{R}	load vector
s	edge length of finite element
T	temperature
T_0	reference temperature for zero stress
t	time
U	conservation variable
u, v	flow velocity components, Eq. (2), or displacement components, Eq. (19)

x, y	coordinate directions
X, Y	principal coordinate directions
Δt	time step
ΔU	$U^{n+1} - U^n$
β	thermal expansion parameter
δ	boundary layer thickness
ϵ	flow total energy, Eq. (2), or strain components, Eq. (18)
λ	eigenvalues
ϕ	key parameter for remeshing, Eq. (20)
ρ	density
$\sigma_x, \sigma_y, \tau_{xy}$	fluid stress components, Eq. (2), or solid stress components, Eq. (7)

Subscripts

F	fluid
L	left element
R	right element
T	thermal
s	structural
1	element internal flux
2	flux across element boundary

Superscripts

I	inviscid
V	viscous
T	transpose
i,j	summation indices
n	time step index, t = nΔt

Introduction

Design of lightweight structures and thermal protection systems for hypersonic vehicles depends on accurate prediction of aerothermal loads, structural temperatures and their gradients, and structural deformations and stresses. Adaptive unstructured remeshing techniques combined with the finite element method have been shown to improve significantly the efficiency and accuracy of the flow analysis. These benefits should accrue for both the thermal and structural analyses of structures. In addition, a universal remeshing procedure is needed for the development of an integrated fluid-thermal-structural analysis capability.

Research is currently underway at NASA Langley Research Center to develop an integrated analysis approach for accurately predicting each disciplinary behavior and their interactions. The approach uses the finite element method to solve: (1) the Navier-Stokes equations for the aerodynamic flow field and the aerothermal loads; (2) the structural energy equation for heat transfer and temperature distribution; and (3) the structural equilibrium equations for deformation and stresses. The capability of the approach was demonstrated for an undisturbed Mach 6 flow over a

*Aerospace Technologist, Aerothermal Loads Branch, Structural Mechanics Division, Member AIAA

three-inch-diameter stainless steel cylinder[1] for which the experimental data[2] were available for comparison. The flow field is characterized by the bow shock that stands-off the cylinder and the thin boundary layer at the cylinder surface. Sharp gradients in the flow variables occur in these regions and closely spaced elements were generated manually to model these flow features. The flow solution compares well with the experimental data demonstrating the effectiveness of the finite element method used.

For a more complex problem, where a priori knowledge of the flow physics does not exist, an appropriate finite element mesh may not be constructed easily. An adaptive mesh generation technique is required not only to construct and adapt the mesh automatically to represent the flow field but also to reduce the number of unknowns and the analysis computational time. Thus the current focus on the improvement of the integrated analysis approach is to develop efficient adaptive unstructured mesh generation techniques for each analysis discipline considered including their interface requirements.

Adaptive mesh generation techniques may be classified into two major categories: (1) refinement/derefinement, and (2) remeshing. The first category, the adaptive refinement/derefinement technique, can be further classified into three subcategories: (a) the h method, (b) the p method, and (c) the r method. In the h method, the elements in the initial mesh are refined into smaller elements or derefined into larger elements[3]. The p method maintains the geometry of the elements of the initial mesh but increases (or decreases) the order of the polynomial used for the element interpolation function[4]. The r method keeps the number of elements and their connectivities the same but relocates the nodes[5]. These methods help increase the analysis solution accuracy but each has limitations. Even though nodes could be added or removed by the h method, the orientation of the original and new elements does not change. Orientation of element sides along principal flow gradients increases solution accuracy and reduces the number of elements[6]. Even though the r method can move the nodes for better alignment, the method may generate highly distorted elements if the number of elements is fixed. The p method may alleviate these restrictions because of the flexibility in selecting the order of polynomials on the element sides. However, the use of such higher order polynomials in combination with the hierarchical concept leads to complexities in the formulation of finite element equations and implementation in computer programs.

The above considerations led to the development of the second adaptive mesh category, the remeshing technique[7]. The technique generates an entirely new mesh based on the solution obtained from the earlier mesh. The technique combined with the finite element method has been applied successfully to several compressible flow problems with complex flow behavior[8,9]. The purpose of this paper is to extend the adaptive remeshing technique to both the thermal and structural analyses of structures. The adaptive remeshing technique will be evaluated to assess its effectiveness for the integrated fluid-thermal-structural analysis. The governing equations for the aerodynamic flow, structural heat transfer, and structural response will be introduced first. The finite element solution algorithms for solving these equations will be described. The

basic concepts of the adaptive remeshing technique will then be explained. Selection of indicators used for construction of new meshes for the three analysis disciplines will be discussed. Finally the adaptive remeshing technique will be evaluated for: (1) the fluid analysis of Mach 8 shock-shock interference on a three-inch-diameter cylinder where the experimental data is available, and (2) the thermal-structural analysis of a 0.25-inch-diameter convectively cooled leading edge subjected to intense aerodynamic heating simulating Mach 16 flight condition. The issues of mesh continuity along the fluid/structure interface and between thermal and structural analyses for direct interdisciplinary data transfer will also be discussed.

Integrated Fluid-Thermal-Structural Procedure

Governing Equations

Aerodynamic Flow. The equations for a laminar compressible flow are governed by the conservation of mass, momentum, and energy. These equations are written in conservation form as

$$\frac{\partial}{\partial t}\{U_F\} + \frac{\partial}{\partial x}\{E_F\} + \frac{\partial}{\partial y}\{F_F\} = 0 \qquad (1)$$

where the subscript F denotes the fluid analysis. The conservation variables vector, $\{U_F\}$, and the flux vectors in the x and y directions, $\{E_F\}$ and $\{F_F\}$, are given by

$$\{U_F\}^T = [\rho \quad \rho u \quad \rho v \quad \rho \varepsilon]$$

$$\begin{aligned}
\{E_F\}^T &= [E_F]^I + [E_F]^V \\
&= [\rho u \quad \rho u^2+p \quad \rho uv \quad \rho u\varepsilon+pu] \\
&\quad - [0 \quad \sigma_x \quad \tau_{xy} \quad u\sigma_x+v\tau_{xy}-q_x]
\end{aligned}$$

$$\begin{aligned}
\{F_F\}^T &= [F_F]^I + [F_F]^V \\
&= [\rho v \quad \rho uv \quad \rho v^2+p \quad \rho v\varepsilon+pv] \\
&\quad - [0 \quad \tau_{xy} \quad \sigma_y \quad u\tau_{xy}+v\sigma_y-q_y] \quad (2)
\end{aligned}$$

Superscripts I and V represent the inviscid and viscous flux vector components, respectively. The pressure p is related to the total energy assuming a calorically perfect gas (constant ratio of specific heats). The stresses σ_x, σ_y, and τ_{xy} are related to the velocity gradients by Stokes' hypothesis. The heat fluxes q_x and q_y are related to the temperature gradients by Fourier's law. The temperature-dependent viscosity is computed from Sutherland's law and the thermal conductivity is computed assuming a constant Prandtl number of 0.72.

Structural Heat Transfer. The thermal response of the structure is governed by the energy equation which is written in conservation form as

$$\frac{\partial}{\partial t}(U_T) + \frac{\partial}{\partial x}(E_T) + \frac{\partial}{\partial y}(F_T) = H_T \qquad (3)$$

where the subscript T denotes thermal analysis. For transient heat conduction, the conservation variable, U_T, and the heat flux components, E_T and F_T, are

$$dU_T = \rho_s c_s dT_s$$

$$E_T = q_x = -k_s \frac{\partial T}{\partial x}$$

$$F_T = q_y = -k_s \frac{\partial T}{\partial y} \qquad (4)$$

and H_T is the heat source. The structural heat flux components q_x and q_y are related to the temperature gradients by Fourier's law.

For a structure with internal convection cooling, the energy equation for the coolant flow in the local x-direction based on assumed uniform cross-sectional or bulk temperature[1] can also be written in the conservation form of Eq. (3) where

$$dU_T = \rho_F c_F dT_F$$

$$E_T = \dot{m} c_F T_F / A_F - k_F \partial T / \partial x$$

$$F_T = 0$$

$$H_T = hP(T_s - T_F) \qquad (5)$$

The flux E_T consists of the energy transport by convection (1st term) and conduction (2nd term), and the flux H_T represents the heat transfer between the structure and the coolant.

Structural Response. The structural response is governed by the quasi-static equilibrium equations assuming that the inertia effect is negligible. These equations are written in conservation form as

$$\frac{\partial}{\partial x}\{E_s\} + \frac{\partial}{\partial y}\{F_s\} = 0 \qquad (6)$$

The flux vector components, $\{E_s\}$ and $\{F_s\}$, are

$$\{E_s\}^T = [\sigma_x \quad \tau_{xy}]$$

$$\{F_s\}^T = [\tau_{xy} \quad \sigma_y] \qquad (7)$$

where the stress components, σ_x, σ_y, and τ_{xy} are related to the displacement gradients and the temperature by generalized Hooke's law.

Finite Element Solution Algorithms

An implicit/explicit upwind cell-centered algorithm[9,10] is used to solve the Navier-Stokes equations, Eqs. (1)-(2). A flux-based Taylor-Galerkin finite element algorithm[9,11] is used to solve the thermal and structural equations, Eqs. (3)-(7). For brevity, only essential features of the algorithms are highlighted herein.

Upwind Fluid Algorithm. The basic concept behind the upwind cell-centered algorithm is to determine the flux across element interfaces by Roe's averaging procedure[12]. The average inviscid flux $\bar{E}^I$ (the "overbar" denotes an average quantity normal to the element interface between the left element, L, and the right element, R) is given by

$$\bar{E}^I = \frac{1}{2}[\bar{E}_L^I + \bar{E}_R^I + |A^*|(U_L - U_R)] \qquad (8)$$

where $|A^*|$ denotes the absolute Jacobian matrix associated with the element flow velocity components and the local speed of sound. Details of the Jacobian matrix A^* are given in Ref. [12].

In the computation of viscous flux components such as the heat flux in the x-direction ($q_x = -k_F \partial T / \partial x$), the element temperature gradient is computed from

$$\frac{\partial T(x,y)}{\partial x} = [N(x,y)]\{\frac{\partial T}{\partial x}\} \qquad (9)$$

where $[N(x,y)]$ is a matrix of finite element interpolation functions. The vector on the right hand side of the equation contains the nodal temperature gradients, determined at node κ, by

$$\frac{\partial T}{\partial x}\big|_\kappa = \frac{1}{M_\kappa}(\int_s \bar{n} T N_\kappa ds - \int_A T \frac{\partial N_\kappa}{\partial x} dA) \qquad (10)$$

where $\bar{n}$ is the unit normal vector along the element interface s and M_κ is the lumped mass at node κ.

Increments in time of the element conservation variables, $\Delta U = U^{n+1} - U^n$, are determined from

$$[[I] + \frac{\Delta t}{A} \sum_s ([A^*]\frac{s}{2} - [B])]\Delta U$$

$$= -\frac{\Delta t}{A}\sum_s s[\bar{E}^I + \bar{E}^V] \qquad (11)$$

The matrix [B], which is associated with the viscous fluxes is given in Ref. [10], accelerates the solution convergence in the viscous dominated regions. This fluid algorithm provides first order of accuracy ($O(h)$) in the inviscid flow dominated region but the order of accuracy is close to 1.5 ($O(h^{1.5})$) in the viscous flow dominated region[10].

Flux-Based Taylor-Galerkin Algorithm. The basic concept of the flux-based Taylor-Galerkin algorithm is to express the element flux components E and F in the form

$$E(x,y,t) = [N(x,y)]\{E(t)\}$$
$$F(x,y,t) = [N(x,y)]\{F(t)\} \qquad (12)$$

where $\{E\}$, and $\{F\}$ are vectors of the element nodal flux quantities.

For the thermal analysis, the final finite element equations are in the form

$$[M]\{\Delta U_T\}^{n+1} = \{R_T\}_1^n + \{R_T\}_2^n \qquad (13)$$

where at time n+1, $\Delta U^{n+1} = U^{n+1} - U^n$. The mass matrix, [M], is determined from

$$[M] = \int_A [N][N] dA \qquad (14)$$

The two vectors on the right hand side of Eq. (13) are associated with the fluxes within the element (subscript

1) and across the element boundary (subscript 2). These vectors are defined by

$$\{R_T\}_1^n = \Delta t \left(\int_A \{ \frac{\partial N}{\partial x} \} [N] dA \{E_T\}^n \right.$$

$$\left. + \int_A \{ \frac{\partial N}{\partial y} \} [N] dA \{F_T\}^n \right) \qquad (15)$$

$$\{R_T\}_2^n = -\Delta t \int_s \{N\}[N] ds \; (l\{E_T\}^n + m\{F_T\}^n)$$

$$= -\Delta t \int_s \{N\}[N] ds \; \{q\}^n \qquad (16)$$

The vectors $\{E_T\}$ and $\{F_T\}$ contain nodal heat fluxes which depend on the nodal temperature gradients. The element nodal temperature gradients $\partial T/\partial x$ and $\partial T/\partial y$, and all the finite element matrices (Eqs. (13)-(16)) can be evaluated in closed form (i.e., numerical integration is not required) for any type of finite elements including the 4-node quadrilateral and the 8-node hexahedral elements.

For the structural analysis, the final finite element equations are in the same form as the thermal equation, Eq. (13), but without the transient term,

$$\{R_s\}_1 + \{R_s\}_2 = 0 \qquad (17)$$

where these vectors are identical to Eqs. (15)-(16) except that the subscript T is replaced by the subscript s everywhere. The element nodal flux vectors $\{E_s\}$ and $\{F_s\}$ (similar to $\{E_T\}$ and $\{F_T\}$ in Eq. (15)) now consist of the stress components σ_x, σ_y and τ_{xy}. By using the thermal stress-strain constitutive relations,

$$\sigma_i = c_{ij} \epsilon_j + \beta_i (T - T_o) \quad i,j = 1,2,3 \qquad (18)$$

and the strain-displacement relations, these nodal stress components associated with the $\{R_s\}_1$ vector can be written in terms of the nodal displacement components. Further algebraic manipulation of the finite element equation, Eq. (17), results in the standard form of

$$[K]\{U\} = \{R_s\}_2 + \{R_T\} \qquad (19)$$

where $\{U\}$ consists of the unknowns of the nodal displacement components, [K] is the element stiffness matrix, and $\{R_T\}$ is the thermal load vector. These matrices are evaluated in closed form and the details are given in Ref. [11].

Adaptive Remeshing Procedure

Remeshing Concept

The basic idea of adaptive remeshing is to construct a completely new mesh based on the solution obtained from the previous mesh. The new mesh will consist of clustered elements in regions with large solution gradients and few elements in the regions where the gradients are small. Element orientations are in principal directions to provide the most accurate solution with a minimum number of elements. As an example, the shorter element side is in the direction normal to the shock line or through the boundary layer thickness to

model large solution gradients. Based on these ideas, the adaptive remeshing technique consists of two steps: (1) the determination of the new element sizes and their orientations, and (2) the construction of the new mesh.

In the determination of the element size and orientation, the solid mechanics concept of determining the principal stresses and their directions from a given state of stress at a point is employed. For example in the thermal analysis, small and clustered elements are needed in regions of large temperature gradients. The temperature is thus considered as a key parameter to indicate where clustered elements are needed. At a typical node in the old mesh, the second derivative[10] of the key parameter with respect to the global coordinates x and y are first computed,

$$\begin{bmatrix} \dfrac{\partial^2 \phi}{\partial x^2} & \dfrac{\partial^2 \phi}{\partial x \partial y} \\[3mm] \dfrac{\partial^2 \phi}{\partial x \partial y} & \dfrac{\partial^2 \phi}{\partial y^2} \end{bmatrix} \qquad (20)$$

where ϕ denotes the key parameter used for remeshing. Then the eigenvalues which represent the principal quantities in the principal directions X and Y where the cross derivatives vanish are determined,

$$\lambda_1 = \left| \frac{\partial^2 \phi}{\partial X^2} \right| \quad \text{and} \quad \lambda_2 = \left| \frac{\partial^2 \phi}{\partial Y^2} \right| \qquad (21)$$

These eigenvalues are the remeshing indicators and are used to determine the element spacings h_1 and h_2 in the two principal directions using the condition of

$$h_1^2 \lambda_1 = h_2^2 \lambda_2 = \text{constant} \qquad (22)$$

which has been shown to distribute the solution error equally, a condition for an optimal mesh[13]. This process is performed for all the nodes in the old mesh leading to the final condition[7] of

$$h_1^2 \lambda_1 = h_2^2 \lambda_2 = \text{constant} = h_{min}^2 \lambda_{max} \qquad (23)$$

Using this condition and specifying the required minimum element spacing h_{min}, the new element spacings based on the solution of the old mesh are obtained and the new mesh is constructed.

Mesh construction is based on an advancing front technique[7]. Nodes are first placed along the domain boundary. Spacings between these nodes are dictated by the element spacing parameter h obtained earlier. At this instance, the front consists of a sequence of straight line segments which connect consecutive boundary nodes, i.e., the domain boundary. Elements adjacent to the domain boundary are then constructed. The sizes and orientations of these elements are guided by the computed element spacing parameter h and the principal directions. As new elements are constructed from the domain boundary, the front is updated and represented by the new element sides. As the mesh construction goes on, the front changes its shape continuously and propagates toward the domain interior. The generation

process is terminated when the domain is filled completely with elements and the front vanishes.

Based on the condition shown in Eq. (23), the element size is generated according to the given minimum element spacing h_{min}. Specifying too small a spacing h_{min} could result in a model with a large number of elements which may be impractical to perform the analysis. On the other hand, specifying too large a spacing h_{min} may result in an inadequate analysis solution accuracy, or excessive analysis and remeshing cycles to achieve the required solution accuracy. These factors must be considered prior to generating a new mesh. Note that, because the technique generates an entirely new mesh with different nodal locations from the old mesh, interpolation of the solution from the old to the new mesh is necessary. The interpolated nodal quantities are used as the initial conditions for the new mesh to increase the analysis solution convergence.

Fluid-Thermal-Structural Remeshing Parameters

The adaptive remeshing technique described requires a selection of proper key parameters (ϕ in Eq. (20)) for remeshing so that generated elements are clustered where needed. Selection of the key parameters depends on the analysis discipline and its applications. For thermal problems, it is obvious that the temperature should be used as the key parameter so that the mesh generated can represent steep temperature gradients. For structural problems, stress is an appropriate choice for the key parameter so that regions with high stress concentration will be represented. However, the key parameter representing the stress should be a scalar quantity such as the Von Mises stress defined by,

$$\sigma_{Von\ Mises} = \frac{1}{\sqrt{2}} \sqrt{ (\sigma_x - \sigma_y)^2 + \sigma_x^2 + \sigma_y^2 + 6\,\tau_{xy}^2 } \quad (24)$$

Note that the key parameter selected for remeshing may vary with applications. For problems that require accurate deformations rather than the stresses, an absolute displacement quantity may be preferred as the key parameter.

For high-speed compressible flow problems, selection of the proper key parameters for remeshing may be more difficult. In the inviscid flow field, the fluid density is normally selected as the key parameter[9] because density exhibits high gradients across shock and flow expansion waves. In the viscous dominated flow regions, such as the boundary layer, other key parameters may be more appropriate. Key parameters of heating rate and skin friction may be used for more accurate analysis prediction of the aerothermal loads. The selection of these key parameters for remeshing in the three different analysis disciplines will be discussed in detail in the next section.

Evaluation of Integrated Analysis and Adaptive Remeshing Procedures

Two applications are presented to assess the adaptive unstructured remeshing procedures for integrated fluid-thermal-structural finite element analysis. The fluid analysis of Mach 8 shock-shock interference on a three-inch-diameter cylinder is used as the first application to illustrate the successful implementation of the adaptive remeshing technique for complex flow and to investigate the meshing issues for the integrated fluid-thermal-structural model. The applicability of the remeshing technique for thermal and structural problems is demonstrated in the second application for a 0.25-inch-diameter convectively cooled leading edge subjected to intense aerodynamic heating. Remeshing parameters for thermal and mechanical stress predictions are identified.

Mach 8 Shock-Shock Interference On a Cylinder

Leading edges of hypersonic vehicles that experience intense stagnation point pressures and heating rates are a significant challenge to the designer. For engine leading edges, such as the cowl shown in Fig. 1, intense aerothermal loads occur when the cowl bow shock is intersected by an oblique shock resulting in a supersonic jet that impinges on the leading edge surface. The experimental configuration (lower left of Fig. 1), which simulates the vehicle forebody and cowl leading edge, was used to define the aerothermal loads[2,14]. The experimental configuration is rotated 180° relative to the vehicle. The schlieren photograph shows the supersonic jet interference pattern impinging on the surface of the cylinder. The interference pattern produces intense local amplification of the pressure and heat transfer rate in the vicinity of the jet impingement. The undisturbed (absence of incident oblique shock and interference pattern) stagnation pressure and heating rate can be amplified by factors from 6 to 30 depending on the shock strength and the free stream Mach number[2,14].

The flow interaction pattern superimposed on the flow computational domain and the three-inch-diameter cylinder is shown schematically in Fig. 2. The inflow conditions above and below the oblique shock are: (1) Mach 8.03 flow at an angle of attack of zero degrees ($\alpha=0°$) and static temperature of 200 °R, and (2) Mach 5.25 flow at an angle of attack of 12.5 degrees ($\alpha=12.5°$) and a static temperature of 430 °R. The supersonic jet impinges on the cylinder surface approximately 22 degrees below the cylinder horizontal center line.

A first mesh shown in Fig. 3 is generated using a background mesh concept described in Ref. [7]. A total of 4192 triangles are generated in the inviscid region and 1568 quadrilateral elements in the boundary layer. The reasons for using quadrilateral elements in the boundary layer will be described in detail below. Using this mesh, the fluid analysis is performed to obtain a flow solution as illustrated by the Mach number contours shown in Fig. 4. Based on this flow solution and the use of the fluid density as the key parameter for remeshing, the second mesh is created as shown in Fig. 3. The flow solution obtained from the first mesh is then interpolated and used as the initial condition for the second mesh. The same procedure is repeated on the subsequent meshes until the converged flow solution is achieved (a total of three meshes in this case).

The Mach number contours shown in Fig. 4 demonstrate the improvement of the solution quality with the adapted meshes. The Mach number distribution obtained from the third mesh shows improved sharpness of the shock interference pattern. The contours show a supersonic jet (Mach number ~ 2) submerged within the subsonic regions between the bow shock and the cylinder. The supersonic flow in the jet terminates

through a nearly normal shock prior to impinging on the cylinder surface.

The analytically predicted surface pressure distribution from the third mesh is compared with the experimentally measured pressures[2] in Fig. 5. The predicted and experimental pressures are normalized by the undisturbed stagnation pressure (p_0 = 10.61 psia). Good agreement between the analytical and experimental results are obtained for the pressure distribution, the peak pressure and its locations. Details of the finite element mesh and the flow temperature in the interaction region are shown in Fig. 6. On both sides of the supersonic jet, the fluid temperature increases abruptly across the bow shocks from a relatively low temperature (200 °R and 430 °R) to approximately 2,700 °R. The temperature gradients in the shock layer (region between the bow shock and the cylinder) are relatively small except in the thin boundary layer where the temperature drops sharply to the cylinder surface temperature of 530 °R. Inside the supersonic jet, the fluid temperature increases slightly from the free stream temperature to approximately 1,000 °R. As the jet stream approaches the cylinder surface, the fluid temperature increases abruptly across the jet normal shock to approximately 3,000 °R in a small stagnation region next to the cylinder surface and drops sharply to the cylinder temperature of 530 °R resulting in high aerodynamic heating rates.

The major difficulty in the fluid analysis is the prediction of the aerodynamic heating rates because a very accurate resolution of the flow temperature gradient normal to the cylinder surface is required. For the undisturbed Mach 8 flow, the predicted stagnation heating rate of approximately 42 Btu/ft^2-sec, which was obtained from a finite element solution[1] and a viscous shock layer solution[15], is lower than the experimental value of 61.7 Btu/ft^2-sec (Ref. [2]). The predicted and the experimental interference heating rates are, therefore, normalized by their respective undisturbed stagnation point heating rates and are compared in Fig. 7. The heating rate distributions are similar and the peak heating rate locations agree. However the predicted peak heating rate amplification is about 60% of that measured from the experiment. This difference may be attributed to several sources including the finite element mesh, the analysis algorithm, and the mathematical model. The finite element mesh near the boundary layer may be inadequate to represent the steep temperature gradients accurately. The flow analysis algorithm, Eqs. (8)-(11), provides an accuracy on the order of the element characteristic length h raised to the 1.5 power ($O(h^{1.5})$). In addition, the fluid flow mathematical model does not account for any turbulence. As discussed in Ref. 2, the higher experimental heating rate may be attributed to free stream turbulence in the test stream which emanates from (1) the turbulent boundary layer on the nozzle and/or (2) shear layers that separate the supersonic jet from the subsonic regions.

As mentioned earlier, layers of quadrilateral elements are used in the boundary layer. Detail of these quadrilateral elements are shown in Fig. 8. The use of a structured mesh of quadrilateral elements in the boundary layer provides several advantages in the flow analysis. One advantage is that slender (high aspect ratio) elements can be used with their longer sides in the flow direction where the solution gradients are small and their shorter sides normal to the surface to model steep solution gradients through the boundary layer thickness.

A second advantage is that the artificial dissipation required for the numerical stability, which could smear the solution gradients, can be controlled easily or turned off completely[16]. Although the boundary layer thickness varies along the cylinder, the thickness (δ = 0.06 inches in Fig. 8) is assumed constant for the purpose of constructing the boundary layer mesh. Across the boundary layer thickness, 32 layers of graduated quadrilateral elements are used with a geometric stretching factor of 1.25. The thickness of the first element at the surface is $1. \times 10^{-5}$ inches and was chosen such that it should model the temperature gradient expected from the experimental heating rate[2].

For general problems, the boundary layer thickness is not known and varies in the flow direction. An approach to estimate the boundary layer thickness using the fluid heat transfer as the key parameter for remeshing has been proposed recently[10]. The approach is illustrated in Fig. 9. The boundary layer thickness, δ, is estimated from the absolute quantity of the heat flux vector, $|\bar{q}|$, which is a maximum at the surface and is insignificant above the edge of the boundary layer. The size and distribution of the quadrilateral element layers are guided by the magnitude of the flow shearing stress (τ_{xy} is proportional to $\partial u/\partial y$) which is a maximum at the cylinder surface and decreases quadratically through the boundary layer thickness. Based on this idea, an adaptive remeshing technique using quadrilateral elements in the boundary layer can be constructed and combined with the current capability of the adaptive remeshing technique for triangular elements in the inviscid flow region.

To generate an integrated fluid-thermal-structural finite element model, the use of common nodes along the fluid/structure interface is preferred[16] as highlighted in Fig. 10. This approach not only permits direct data transfer between the different analysis disciplines but also provides consistency for the analysis formulation. As an example of a coupled fluid/thermal problem, the interface nodal temperatures can be obtained by solving the coupled energy equation of the flow and the structure[1] with the requirements that at the interface: (1) the temperatures of the fluid and the structure are identical, and (2) the heat flux is continuous.

For some problems, the requirement of common fluid/structure interface nodes to preserve the mesh continuity may result in an excessive number of nodes in one of the disciplines. For example, a high stress concentration may occur near the fluid/structure interface which may require a large number of the structural nodes even though the flow near that region is simple. Several adaptive meshing techniques are feasible for the thermal-structural analysis of the structure as indicated in Fig. 10 which include the mesh refinement/derefinement technique and the remeshing technique developed for the flow problems. Before selecting one of these techniques, their effectiveness for thermal and structural problems must be evaluated. An initial evaluation of the adaptive remeshing technique for both the thermal and structural analyses is performed in the next section.

Convectively Cooled Leading Edge

A 0.25-inch-diameter convectively cooled leading edge subjected to intense aerodynamic heating is used to evaluate the adaptive remeshing technique for both the thermal and structural analyses, and to identify

requirements for the remeshing parameters for thermal stress problems. The example problem represents a hypersonic vehicle operating at Mach 16 which causes the vehicle nose bow shock to intersect with the cowl leading edge bow shock. The intersection produces the type IV supersonic jet interference pattern similar to that described in the first application. Because of the smaller leading edge diameter and the higher Mach number conditions, the heating rate is very intense with a peak of nearly 30,000 Btu/ft^2-sec (see Ref. [1]).

The leading edge geometry and boundary conditions are shown schematically in Fig. 11. The outer surface is subjected to the aerodynamic heating and emits radiant energy to space. The inner surface is convectively cooled by the direct impingement of a sonic hydrogen jet stream with an inlet temperature of 50 °R. The 1350 quadrilateral element mesh shown in Fig. 12(a) is typical of a structured mesh. The mesh has been used previously[1] for predicting transient thermal-structural response of the leading edge as the vehicle nose bow shock sweeps across during the vehicle acceleration. The mesh is graded in the radial direction but is uniform in the circumferential direction. The leading edge material is assumed to be copper because of its high thermal conductivity. The copper material properties used in the analysis are highly temperature dependent and can be found in Refs. [17-18]. The predicted steady-state leading edge temperature contours are shown in Fig. 12(b). The peak temperature of 766 °R is at the jet impingement location where the heating rate is a maximum. In spite of the high thermal conductivity of the material, the temperature gradients are also high in this region. The problem is, therefore, suitable to be used for evaluating the adaptive remeshing technique for the thermal analysis of the structure.

The same adaptive remeshing procedure described for the flow problem is applied for the thermal analysis of the leading edge. A fairly uniform mesh consisting of 885 triangles, shown in Fig. 13(a), is first constructed and the thermal analysis is performed to obtain the temperature distribution. Then the adaptive mesh shown in Fig. 13(b) is generated using the temperature as the key parameter for remeshing to provide clustered elements in the region with high temperature gradients. The temperature distribution obtained from the second mesh is almost identical (a difference of 0.2%) to that obtained from the nonadaptive mesh shown in Fig. 12(b). However, the number of unknowns required for the adaptive unstructured mesh is reduce to about 25% of those used in the structured mesh. Note also that several elements are required through the thickness where the peak heating occurs and only one or two elements are required near the end of the leading edge. Hence, only an unstructured mesh technique would optimize the mesh.

To evaluate the effectiveness of the adaptive remeshing technique to represent both the thermal and mechanical stress fields, structural boundary constraints at the upper and lower leading edge sections are introduced. The inner surface nodes at the constraint are fixed (u = v = 0, see Fig. 14(a)) to simulate the constraints caused by the internal fins that support the leading edge from the inner primary structure. To highlight the remeshing capability for generating clustered elements in the regions needed, the rest of the nodes on both sections are constrained differently. These nodes are free to move on the upper section, but are constrained in

the horizontal direction on the lower section. In addition to the thermal loads, the leading edge is also subjected to mechanical loads from: (1) the aerodynamic pressure which has a distribution similar to that shown in Fig. 5 but with a peak pressure of 1,000 psia, and (2) the uniform internal coolant pressure of 1,000 psia.

The adaptive thermal mesh shown in Fig. 13(b) is used as the initial mesh for the structural analysis. The same analysis procedure is applied by first obtaining the structural analysis solution and then remeshing. In the remeshing process, nodal temperatures of the new mesh are interpolated from the nodal temperatures of the thermal mesh shown in Fig. 13(b). For thermal stress problems, high stresses normally occur in regions of high temperature gradients. High stress concentrations may also occur at corners or supports even though the temperature is uniform. Thus, to represent both the thermal stress and the stress concentration, key parameters for remeshing based on the temperature and the Von Mises stress are used. A new adaptive mesh generated by using these two remeshing parameters is shown in Fig. 14(a). Elements are clustered near the jet impingement location for modeling high thermal stresses from the high temperature gradients, and at the region near the upper support where the stress concentration occurs. The corresponding structural response, based on a linear elastic behavior assumption, is shown by the circumferential stress contours superimposed on the deformed leading edge in Fig. 14(b). The figure shows that a peak compressive stress of 25 ksi occurs at the jet impingement location and a high stress concentration occurs near the singular point at the upper support.

To support the idea that the two remeshing parameters should be used simultaneously for generating an adaptive mesh for thermal stress problems, the same analysis approach is repeated but without using the temperature as the remeshing parameter. The adaptive mesh generated using the Von Mises stress alone as the remeshing parameter is shown in Fig. 15(a). Clustered elements are generated in the region near the upper support similar to the previous case. The mesh near the jet impingement location is much coarser than the mesh for the previous case and does not resemble the mesh for the temperature distribution. The corresponding predicted structural response of the circumferential stress contours is shown in Fig. 15(b). The contours are similar to those obtained in the previous case but are degraded due to the coarser mesh in the region of the jet impingement location. The difference between the peak compressive stresses of these two cases at the jet impingement location is approximately 15%. Note that for thermal stress problems in which the structure is free to expand, the thermal stress distribution normally resembles the distribution of the temperature. For such cases, the use of the Von Mises stress alone as the remeshing parameter may be adequate.

The adaptive remeshing technique for the structural analysis is further evaluated for the case in which the thermal load is not present. The leading edge is subjected only to the mechanical load which consists of the external aerodynamic pressure and the internal coolant pressure. The Von Mises stress is used as the remeshing parameter and the adaptive mesh generated is shown in Fig. 16(a). Similar to the previous case, clustered elements are in the region near the upper support where the stress concentration occurs. The corresponding predicted structural response of the circumferential stress contours is shown in Fig. 16(b).

The predicted compressive stress of 5 ksi at the jet impingement location is much lower than the stress that occurred for the case with the thermal load. Obviously, superposition of the results for separate mechanical and thermal stress analyses would require interpolation of the results. Hence, the adaptive remeshing and analysis should be used for the combined load case.

For coupled fluid-thermal-structural analysis, both the thermal and structural response of the leading edge affect the flow field. The flow field has to be updated to include the effects of: (1) the change of the leading edge surface temperature, and (2) the leading edge deformation. The leading edge may deform into or away from the initial flow field and updating the flow computational domain is necessary. The new flow field may govern regions previously occupied by the leading edge where the flow information does not exist. These are some of the future issues which will be encountered and have to be clarified prior to applying the adaptive remeshing technique to coupled interdisciplinary problems

Concluding Remarks

An adaptive unstructured remeshing technique was evaluated for integrated fluid-thermal-structural analysis. The technique generates an entirely new mesh based on the solution obtained from a previous mesh. The new mesh consists of clustered elements in the regions with high solution gradients and few elements in the regions where the gradients are small. The capability of the remeshing technique was demonstrated for the fluid, thermal, and structural analyses. The finite element formulations used for the three disciplines were presented. The basic idea behind the remeshing technique was described and the remeshing indicators and requirements were identified.

Two applications were presented to assess the effectiveness of the remeshing technique. The fluid analysis of Mach 8 shock-shock interference on a three-inch-diameter cylinder was used as the first application to illustrate the remeshing technique for complex flow and to investigate the meshing issues for the integrated fluid-thermal-structural analysis. Fluid density was used as the remeshing parameter for generating adaptive triangular elements in the inviscid flow region. In the current procedure, layers of quadrilateral elements are constructed in the boundary layer to represent accurate aerothermal loads. The predicted aerodynamic pressure and heating rate are in good to fair agreement with the experimental data. An approach for generating an adaptive structured mesh of quadrilateral elements in the boundary layer was described. The approach can be combined with the current adaptive unstructured remeshing technique used in the inviscid region to achieve an automated remeshing capability for the entire flow domain.

The remeshing technique was extended to the thermal and structural analyses of the structure. The applicability of the technique to thermal stress problems was demonstrated with a 0.25-inch-diameter convectively cooled leading edge subjected to intense aerodynamic heating. Temperature was selected as the remeshing parameter in the thermal analysis so that clustered elements are generated in regions of high temperature gradients. The technique provides the same temperature solution accuracy compared to a refined structured mesh but with a significant reduction

in the number of unknowns. For the structural analysis of the leading edge subjected to both thermal and pressure loads, remeshing parameters of the temperature and the Von Mises stress are used to provide clustered elements in regions of high thermal and mechanical stresses as well as regions with a stress concentration.

The results from the applications have demonstrated the viability of the adaptive unstructured remeshing technique combined with the finite element methods to provide efficient accurate solutions to complex flow-thermal-structural behavior.

References

1. Dechaumphal, P., Thornton, E. A. and Wieting, A. R., "Flow-Thermal-Structural Study of Aerodynamically Heated Leading Edges," AIAA Journal of Spacecraft and Rockets, Vol. 26, No. 4, July 1989, pp. 201-209.

2. Wieting, A. R., "Experimental Study of Shock Wave Interference Heating on a Cylinder Leading Edge," NASA TM-100484, May 1987.

3. Ramakrishnan, R., Bey, K. S. and Thornton, E. A., "An Adaptive Quadrilateral and Triangular Finite Element Scheme for Compressible Flows," AIAA Paper No. 88-0033, January 1988.

4. Thornton, E. A. and Dechaumphai, P., "Adaptive Refinement for Effective Finite Element Thermal and Structural Analyses," International Conference on Accuracy Estimates and Adaptive Refinements in Finite Element Computations, Lisbon, Portugal, Vol. 2, 1984, pp. 65-74.

5. Lohner, R., Morgan, K. and Zienkiewicz, O. C., "Adaptive Grid Refinement for Compressible Euler and Navier-Stokes Equations," International Conference on Accuracy Estimates and Adaptive Refinements in Finite Element Computations, Lisbon, Portugal, Vol. 2, 1984, pp. 189-202.

6. Morgan, K., Peraire, J., Thareja, R. R. and Stewart, J. R., "An Adaptive Finite Element Scheme for Euler and Navier-Stokes Equations," AIAA Paper No. 87-1172, June 1987.

7. Peraire, J., Vahdati, M., Morgan, K. and Zienkiewicz, O. C., "Adaptive Remeshing for Compressible Flow Computations," Journal of Computational Physics, Vol. 72, 1987, pp. 449-466.

8. Dechaumphai, P. and Wieting, A. R., "Coupled Fluid-Thermal-Structural Analysis for Aerodynamically Heated Structures," Finite Element Analysis in Fluids, Edited by Chung, T. J. and Karr, G. R., The University of Alabama in Huntsville Press, April 1989, pp. 165-171.

9. Dechaumphai, P., Wieting, A. R. and Pandey, A. K., "Fluid-Thermal-Structural Interaction of Aerodynamically Heated Leading Edges," AIAA Paper No. 89-1227-CP, April 1989.

10. Vemaganti, G. R., "An Adaptive Remeshing Finite Element Method for High Speed Compressible

Flows Using Quadrilateral and Triangular Elements," Ph.D. Dissertation, Old Dominion University, May 1989.

11. Pandey, A. K., Dechaumphai, P. and Wieting, A. R., "Thermal-Structural Finite Element Analysis Using Linear Flux Formulation," AIAA Paper No. 89-1224-CP, April 1989.

12. Gnoffo, P. A., "Application of Program LAURA to Three-Dimensional AOTV Flowfields," AIAA Paper No. 86-0565, January 1986.

13. Oden, J. T. and Carey, G. F., Finite Elements: Mathematical Aspects, Prentice-Hall, Englewood Cliffs, 1981.

14. Holden, M. S., Wieting, A. R., Moselle, J. R. and Glass, C., "Study of Aerothermal Loads Generated in Region of Shock/Shock Interaction in Hypersonic Flow," AIAA Paper No. 88-0477, January 1988.

15. Holcomb, J. E., Curtis, J. T. and Shope, F. L., "A New Version of the CVEQ Hemisphere Viscous Shock Layer Program for Equilibrium Air," Arnold Engineering Development Center, Arnold Air Force Station, TN, AEDC-TMR-85-V7, February 1985.

16. Thornton, E. A. and Dechaumphai, P., "Coupled Flow, Thermal, and Structural Analyses of Aerodynamically Heated Panels," AIAA Journal of Aircraft, Vol. 25, No. 11, November 1988, pp. 1052-1059.

17. Touloukian, Y. S., Powell, R. W., Ho, C. Y. and Klemens, P. G., "Thermal Conductivity for Metallic Elements and Alloys," Thermophysical Properties of Matters, Vol.1, IFI/Plenum, New York, 1970, pp. 68-81.

18. Metals Handbook Committee: Metal Handbook, Eight Edition, American Society for Metals, Ohio, 1975.

Fig. 2 Oblique and bow shock interaction pattern for Mach 8 shock-shock interference on a three-inch-diameter cylinder.
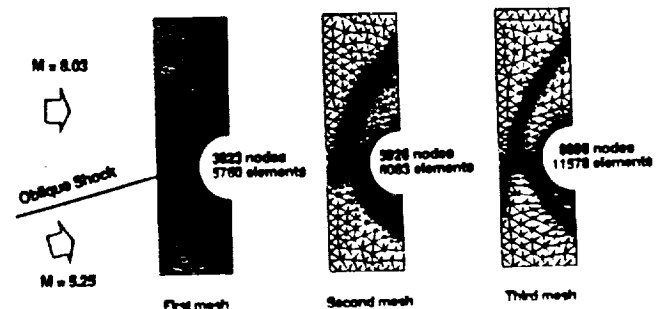
Fig. 3 Adaptive finite element mesh evolution of the flow domain for Mach 8 shock-shock interference on a three-inch-diameter cylinder.

Fig. 1 Vehicle schematic, experimental configuration, and schlieren of type IV shock-shock interference.
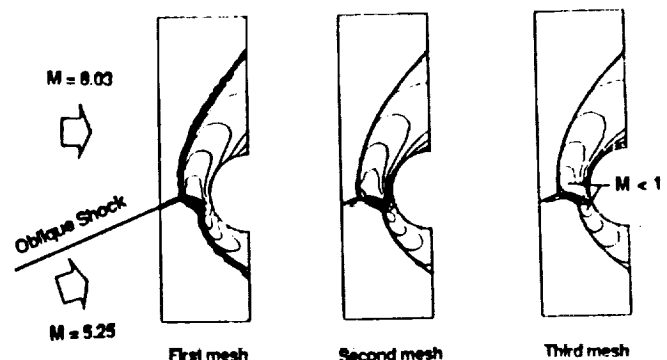

Fig. 4 Flow Mach number contours for the three adaptive unstructured finite element meshes for Mach 8 shock-shock interference on a three-inch-diameter cylinder.
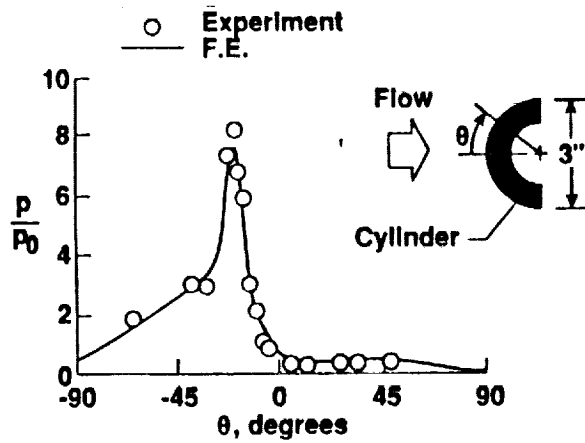
9

Fig. 5 Comparison of surface pressure distributions on a three-inch-diameter cylinder subjected to Mach 8 shock-shock interference.
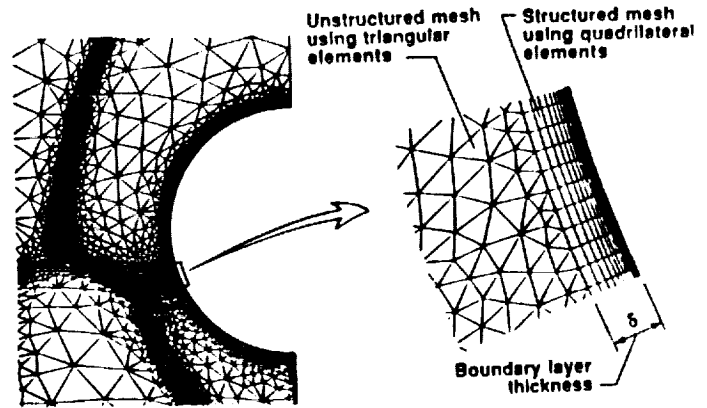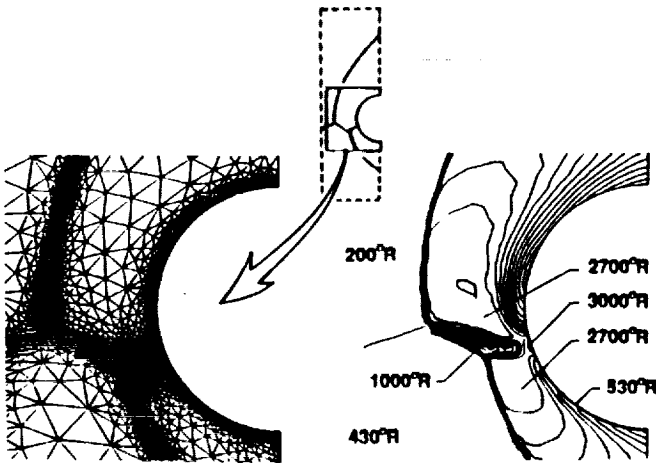

Fig. 6 Details of the finite element mesh and fluid temperature contours in the interaction region for Mach 8 shock-shock interference on a three-inch-diameter cylinder.
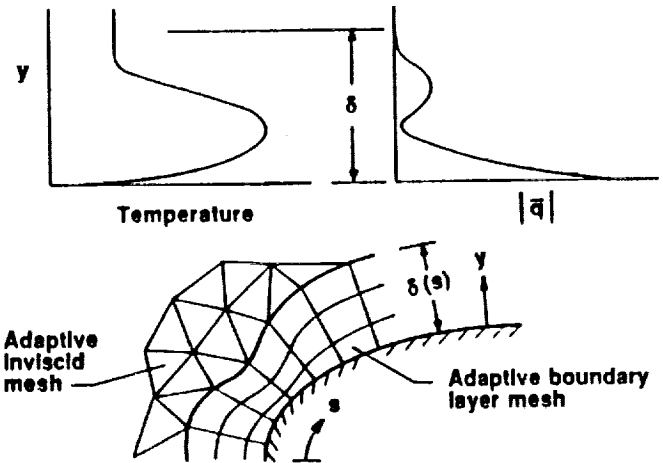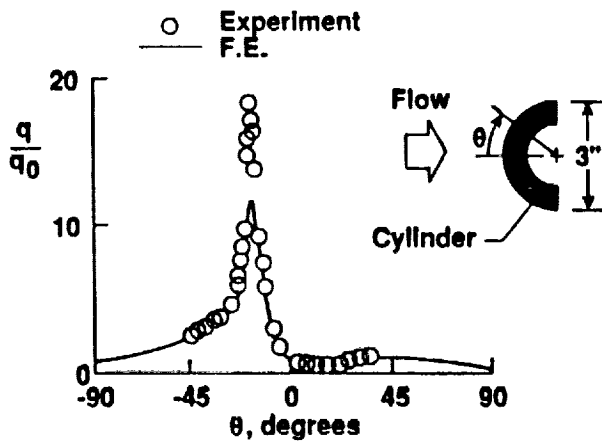

Fig. 7 Comparison of surface heating rate distributions on a three-inch-diameter cylinder subjected to Mach 8 shock-shock interference.

Fig. 8 Details of the finite element mesh in the interaction region and layers of quadrilateral elements in the boundary layer.

Fig. 9 Typical temperature and absolute heat flux vector distributions in the boundary layer and adaptive boundary layer mesh with quadrilateral elements.
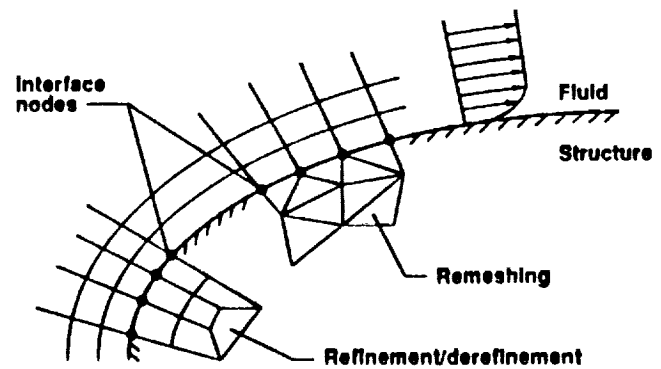

Fig. 10 Integrated fluid-thermal-structural mesh concept and adaptive meshing options for thermal-structural analysis of the structure.
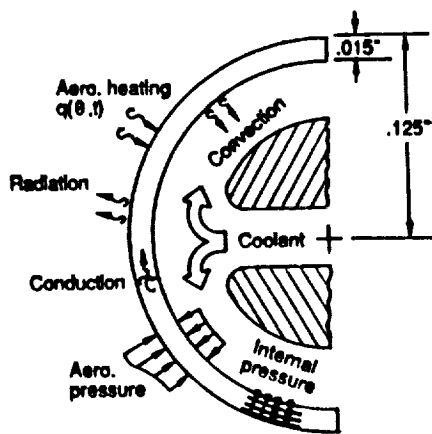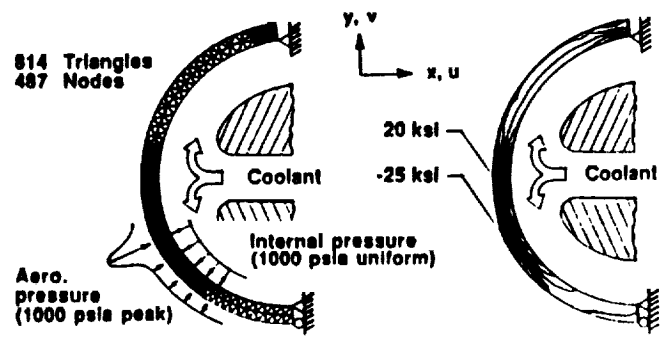
10

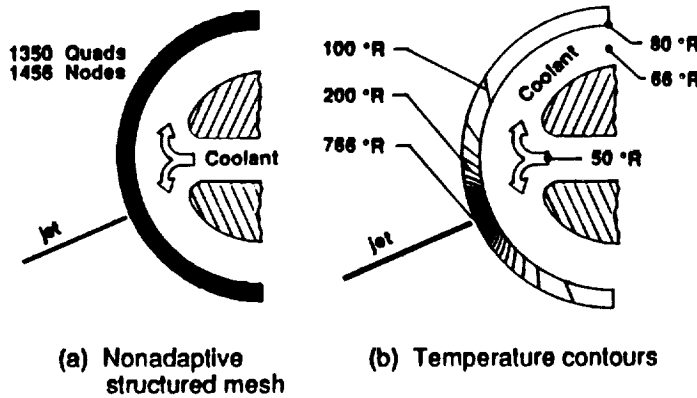**Fig. 11** A schematic thermal-structural analysis model of 0.25-inch-diameter leading edge with boundary conditions.


(a) Nonadaptive structured mesh   (b) Temperature contours

Fig. 12 Nonadaptive finite element mesh and temperature contours for convectively cooled leading edge.

(a) First mesh   (b) Second mesh

Fig. 13 Adaptive finite element mesh evolution for thermal analysis of convectively cooled leading edge.

(a) Adaptive mesh   (b) Circumferential stress

Fig. 14 Final adaptive mesh and circumferential stress for convectively cooled leading edge subjected to thermal and pressure loads.
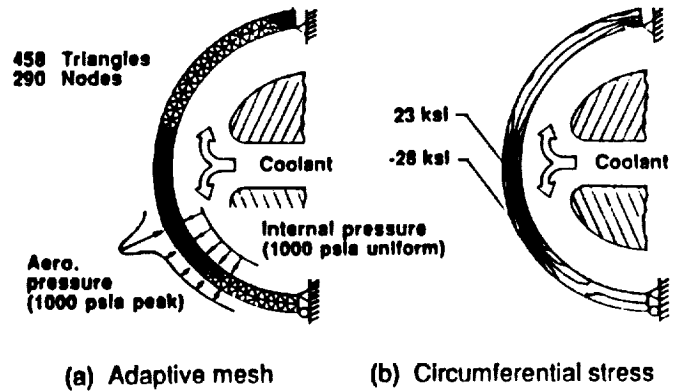
(a) Adaptive mesh   (b) Circumferential stress

Fig. 15 Adaptive mesh using indicator of Von Mises stress and circumferential stress for convectively cooled leading edge subjected to thermal and pressure loads.
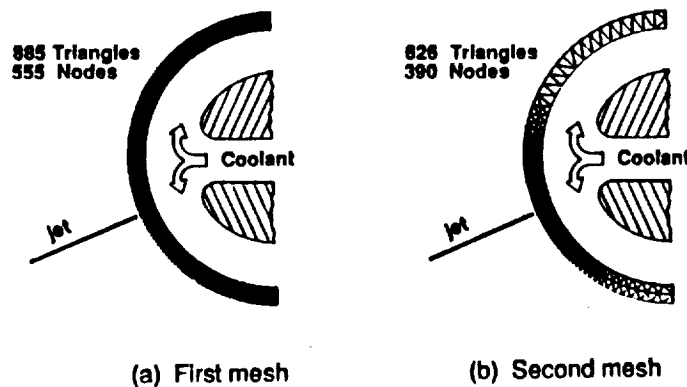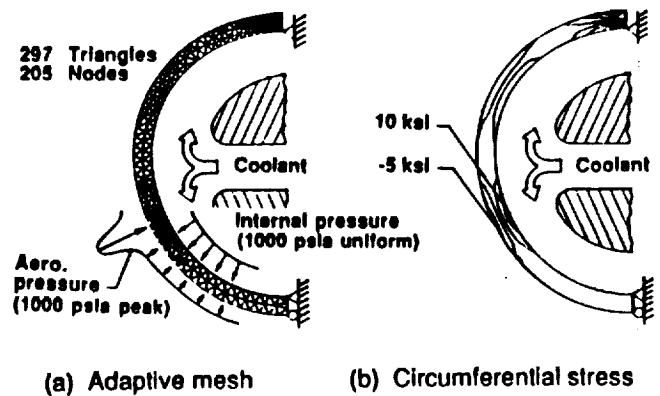

(a) Adaptive mesh   (b) Circumferential stress

Fig. 16 Final adaptive mesh and circumferential stress for convectively cooled leading edge subjected to pressure load.

11

Report Documentation Page

1. Report No. NASA TM-102611	2. Government Accession No.	3. Recipient's Catalog No.
4. Title and Subtitle Evaluation of an Adaptive Unstructured Remeshing Technique for Integrated Fluid-Thermal-Structural Analysis		**5. Report Date** February 1990
		6. Performing Organization Code
7. Author(s) Pramote Dechaumphai		**8. Performing Organization Report No.**
		10. Work Unit No. 506-43-31-05
9. Performing Organization Name and Address Langley Research Center Hampton, VA 23665-5225		**11. Contract or Grant No.**
		13. Type of Report and Period Covered Technical Memorandum
12. Sponsoring Agency Name and Address National Aeronautics and Space Administration Washington, DC 20546-0001		**14. Sponsoring Agency Code**

15. Supplementary Notes

Presented to AIAA 28th Aerospace Sciences Meeting, Reno, Nevada, January 8-11, 1990

16. Abstract

An adaptive unstructured remeshing technique is evaluated for integrated fluid-thermal-structural analysis. The technique is combined with the finite element method to solve: (1) the Navier-Stokes equations for high-speed compressible flow, (2) the energy equation for the structural-thermal response, and (3) the quasistatic equilibrium equations for the structural response. The remeshing technique and the analysis solution procedure are described. The effectiveness of the approach is evaluated with two application studies. The flow analysis of Mach 8 shock-shock interference on a three-inch diameter cylinder is used as the first application study to demonstrate the capability of the remeshing technique and to examine proper remeshing indicators for the inviscid and boundary layer regions. The applicability of the approach for the thermal and structural analyses of the structure is evaluated in the second application study of a 0.25-inch diameter convectively cooled leading edge subjected to intense aerodynamic heating. Issues associated with remeshing indicators for thermal stress problems are identified.

17. Key Words (Suggested by Author(s)) High Speed Flows Aerodynamic Heating Thermal Stress Finite Element		18. Distribution Statement Unclassified - Unlimited Subject Category - 39	
19. Security Classif. (of this report) Unclassified	**20. Security Classif. (of this page)** Unclassified	**21. No. of pages** 12	**22. Price** A03